analytical chemistry

Article

Shotgun Lipidomic Profiling of the NCI60 Cell Line Panel Using Rapid Evaporative Ionization Mass Spectrometry

Nicole Strittmatter, Anna Lovrics, Judit Sessler, James S McKenzie, Zsolt Bodai, M. Luisa Doria, Nora Kucsma, Gergely Szakacs, and Zoltan Takats

Anal. Chem., **Just Accepted Manuscript** • DOI: 10.1021/acs.analchem.6b00187 • Publication Date (Web): 05 Jul 2016

ACS Publications

Analytical Chemistry is published by the American Chemical Society. 1155 Sixteenth Street N.W., Washington, DC 20036

Shotgun Lipidomic Profiling of the NCI60 Cell Line Panel Using Rapid Evaporative Ionization Mass Spectrometry

Nicole Strittmatter[1, ‡,†], Anna Lovrics[2, ‡], Judit Sessler[2], James S. McKenzie[1], Zsolt Bodai[1], M. Luisa Doria[1], Nora Kucsma[2], Gergely Szakacs[2,3,*], Zoltan Takats[1,*]

1: Department of Surgery and Cancer, Imperial College London, London SW7 2AZ, UK

2: Institute of Enzymology, Research Centre for Natural Sciences, Hungarian Academy of Sciences, 1113 Budapest, Hungary

3: Institute of Cancer Research, Department of Medicine I, Comprehensive Cancer Center, Medical University of Vienna, 1090 Vienna, Austria

ABSTRACT: Rapid Evaporative Ionization Mass Spectrometry (REIMS) was used for the rapid mass spectrometric profiling of cancer cell lines. Spectral reproducibility was assessed for three different cell lines and extent of inter-class differences and intra-class variance were found to allow the identification of these cell lines based on the REIMS data. Subsequently, the NCI60 cell line panel was subjected to REIMS analysis and the resulting dataset was investigated for its distinction of individual cell lines and different tissue types of origin. Information content of REIMS spectral profiles of cell lines were found to be similar to those obtained of mammalian tissues although pronounced differences in relative lipid intensity were observed. Ultimately, REIMS was shown to detect changes in lipid content of cell lines due to Mycoplasma infection. The data show that REIMS is an attractive means to study cell lines involving minimal sample preparation and analysis times in the range of seconds.

INTRODUCTION

Rapid Evaporative Ionization Mass Spectrometry (REIMS) is an ambient mass spectrometric method, which was recently developed for intra-operative tissue identification.[1,2] In case of REIMS analysis, biological samples are rapidly heated up via Joule-heating and the resulting aerosol is directly transferred into the mass spectrometer. It was found that electrosurgical tools such as monopolar diathermy that are used in many open surgeries or the bipolar forceps as commonly applied in brain surgery can serve as ion sources following the REI (rapid evaporation ionization) mechanism. A chemical fingerprint of the sample is recorded by the mass spectrometric analysis of the charged particles carried by the aerosol created during ionization. REIMS profiles mainly display complex phospholipid species originating from the cell membranes and were shown to be highly specific to the histological or histopathological type of the tissues.[1] More recently, we further developed the REIMS methodology to characterize and identify microorganisms including bacteria and fungi with excellent accuracies on species-, genus- and Gram-level. REIMS profiles showed sufficient specificity to allow strain-level differentiation of seven *Escherichia coli* strains with an overall 88% accuracy independent of culturing conditions or the age of colonies.[3]

This study on microorganisms and earlier studies on mammalian tissues revealed that the information content of the REIMS spectral profiles is not limited to species-level identification and tissue morphologies but contains additional information on the phenotype of the organism examined.[1,3] REIMS can therefore serve as a lipidomics-based shotgun phenotyping technique, however, the general sensitivity and specificity of the method to certain changes (as changes in protein expression patterns) in a biological system still need to be assessed.

The traditional technique of choice for lipidomic profiling is liquid chromatography-mass spectrometry (LC-MS). However, even using state-of-the-art ultra-high performance liquid chromatography mass spectrometry (UPLC-MS), overall run-time per sample is still in the range of 10-20 minutes and the analysis requires extensive sample preparation (homogenization, extraction, etc.). Several mass spectrometric profiling methodologies have been developed in the recent past and the field has gained additional momentum with the introduction of ambient mass spectrometry in 2004.[4,5] Ambient mass spectrometric methods such as the most widely used Desorption Electrospray Ionization Mass Spectrometry (DESI-MS), offer the capabilities to analyze samples in their native state, without any significant sample preparation steps.[6] These ambient profiling technologies have recently been deployed in cancer studies to characterize the lipid composition of breast cancer compared to normal breast tissue[7], the identification of cancer metastasis within lymph nodes[8], colorectal cancer compared to normal mucosa[9], and brain cancer[10] among others. While these studies provided excellent basis for the development of novel diagnostic approaches, the molecular background of the distinction between different histological classes remains unclear, due to the limited coverage of tissue metabolome/lipidome/proteome and lack of functional tests (e.g. gene silencing) in case of human samples. A complementary approach for studying the molecular background of histologically specific lipid profiles involves the use of cell lines, which solves problems regarding sample availability and standardization of sampling, lifts most of the

ethical constraints and also allows functional testing including gene silencing or metabolic flux analysis.

Cell lines are a popular means of studying various biochemical and disease processes *in vitro*. In case of cancer studies the cell lines provide a means to study cancer development and progression as well as the investigation of pathobiochemical processes as close to the human body as possible while still allowing free manipulation of experimental parameters. One of the most extensively characterized cell line collections is the NCI60 cell line panel which was compiled by the National Cancer Institute as part of the In Vitro Cell Line Screening Project.[11] The panel comprises 60 human cancerous cell lines from nine different organs of origin, namely leukemia, melanoma, cancers of the lung, colon, brain, ovary, breast, prostate, and kidney. Data available for these cell lines includes drug sensitivity patterns for more than 100,000 compounds and natural products, global protein and gene expression data and common mutations associated with cancer.[11-14] However, the associated metabolomics and lipidomics data is comparatively sparse. Although many publications are available investigating the lipid composition of certain types of cell lines using both chromatography-based[15,16] and shotgun mass spectrometry methods,[4,17-20] to our knowledge there is no work available characterizing the lipidome of the NCI60 cell line panel as a whole using a single set of conditions. This represents a striking gap in the cancer-related biochemical data, as complex lipids are the main constituents of cell membranes and play important functional, structural, and metabolic roles by acting as signaling molecules or as precursors for secondary messengers. Furthermore, changes in the membrane lipid composition can regulate function and availability of intrinsic membrane proteins and affect cell signaling mechanisms. REIMS, as other ambient ionization technologies (or desorption ionization technologies in general), yields abundant phospholipid signals due to the good ionization efficiency of polar lipids and their high abundance in biological tissues.

Using REIMS, the objective of the current study is to establish and characterize the methodological background for acquiring shotgun lipid profiling data of large cell line cohorts such as the NCI60 cell line panel. Such methodology will aid future fundamental studies aimed at the exploration of the molecular background of intra-operative REIMS-based tissue identification.

MATERIALS AND METHODS

Culturing of cell lines. The NCI60 cell panel was obtained from the DCTD Tumor Repository (National Cancer Institute, Frederick, MD, USA); HEK, HeLA and MES-SA cell lines were from the ATCC collection (Manassas, VA, USA). All cells were cultured in RPMI 1640 medium with the exception of HEK and HeLa cells in the Mycoplasma study which were cultured in Gibco DMEM medium (Invitrogen, Carlsbad, CA, USA). In all cases, media were supplemented with 10% (*v*/*v*) fetal bovine serum, 2mM glutamine, 100 units/mL penicillin, and 100mg/mL streptomycin (Invitrogen). Cells were incubated in 75cm^2 tissue culture flasks under conditions of humidified 37°C, 5% carbon dioxide atmosphere. Cell lines were regularly screened for Mycoplasma contamination using the MycoAlert™ Mycoplasma Detection Kit (Lonza Group Ltd, Basel Switzerland).

At 80-90% confluence, cells were rinsed with Phosphate Buffered Saline (PBS, pH: 7.2) and detached using 0.1% trypsin/EDTA for 10 minutes. While scraped cells can also be analyzed by REIMS (and were used for initial analyses) Trypsin digestion prior to cell pelleting has been used in other lipid profiling studies of cells[21,22] and were used for larger arms of the study as they offer easier automation for cell harvesting.[21,22] The trypsin was subsequently neutralized with excess culture medium. The cell suspensions were centrifuged at 250×g for five minutes. After centrifugation the cells were re-suspended and washed two times in 10mL PBS. A third wash was performed in an Eppendorf tube with only 1mL PBS. The cell pellets were frozen and stored at -80°C until further analysis.

Mycoplasma infection and treatment. Mycoplasma-infected HEK and HeLa cell lines were treated with 25µg/mL Plasmocin™ Mycoplasma Elimination Reagent (InvivoGen, San Diego, CA, USA) for 14 days.

REIMS analysis. For REIMS analysis, two handheld electrodes in form of a forceps were used as the sampling probe (irrigated bipolar forceps, obtained from Erbe Elektromedizin, Tübingen, Germany). A Valleylab Force EZc power-controlled electrosurgical unit (Covidien, Dublin, Ireland) was used at 60 W power setting in bipolar mode as radiofrequency alternating current power supply (470 kHz, sinusoidal). An approximately 1.5 m long 1/8 inch outer diameter, 1/16 inch inner diameter PTFE tubing (Fluidflon PTFE tubing; LIQUID-scan GmbH Co. KG, Überlingen, Germany) was employed to connect the embedded fluid transfer line of the bipolar forceps with the inlet capillary of a Thermo Exactive instrument (Thermo Scientific GmbH, Bremen, Germany). The inherent vacuum system of the mass spectrometer was used for aspiration of the analyte-containing aerosol created during analysis. This setup is adapted from earlier studies on microorganisms[3] and shown in Figure 1 while instrumental settings are given in Table S-1.

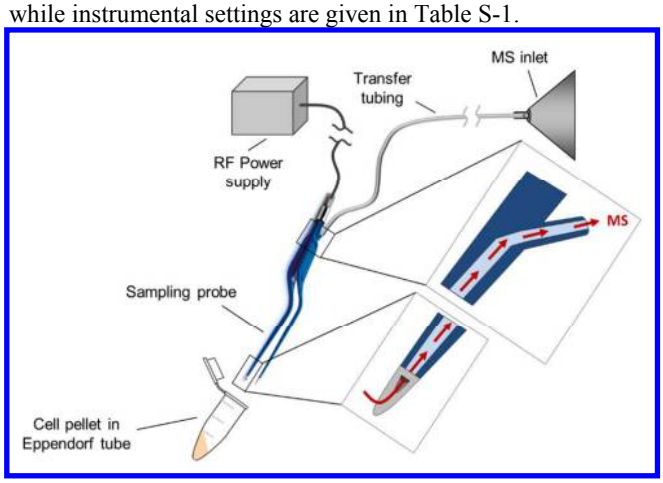

Figure 1. Experimental setup used in this study for REIMS analysis of cell lines. Generated aerosol is sampled via the aspiration port in the head of the sampling probe and transported directly to the mass spectrometer using polymer tubing.

Mass spectrometric analysis of the cell line biomass was performed directly on the thawed cell pellet without further sample pre-processing steps. For each measurement, 0.1-1.5mg of cell biomass was taken up between the tips of the forceps and the two electrodes were subsequently brought into close proximity (i.e. by pinching the biomass between the tips

of the forceps); the RF power supply was triggered using a foot switch. The cell line biomass is rapidly heated up due to its non-zero impedance and an aerosol containing charged molecular species of the analytes is produced and transferred directly into the mass spectrometer. Multiple technical replicates were recorded for each cell line. Ionic species in the mass spectra were identified based on exact mass measurements (mass deviation <3ppm) and MS/MS fragmentation patterns.

Data Analysis. Raw mass spectrometric files were converted into mzML format using the MSConvert tool (part of the ProteoWizard suite, version 3.0.4043) and subsequently imported as imzML format into MATLAB (Mathworks, Natick, MA; http://www.mathworks.co.uk/) for data pre-processing.[3,23,24] All REIMS spectra were linearly interpolated to a common sampling interval of 0.01 Da. Recursive segment-wise peak alignment was then used to remove small mass shifts in peak positions across spectral profiles.[25] The aligned data were subjected to total ion count (TIC) data normalization and log-based transformation. Pattern recognition analysis and visualization were performed either in Matlab or in RStudio (Boston, MA, USA, see also www.r-project.com).[26] The mass range of *m/z* 150-1000 was used for data analysis in all studies. For self-identity experiments, the data set was filtered to keep a reduced set of *m/z* values: a *m/z* value was kept, if the difference between the available samples were significantly different at alpha=0.01 threshold level based on the Kruskal-Wallis test. For each cross-validation run, a principal component analysis (PCA) transformation of the training data set with pre-determined number of principal components (PCs) was calculated in R and prediction score was calculated for each test sample using the 3 nearest neighbor (3-NN) method. The training data in the 'spectral reproducibility set' was selected as follows: for each measurement day, a cell line with defined passage (p) and flask number (A/B) was kept as part of the training data (i. e. HeLa p4 A) if samples were available from at least two different biological replicates (i.e. A1-3). Such sets from each of the three cell lines were combined randomly to produce balanced training data where each cell line is represented by similar number of samples. All of the remaining samples constituted the test set. In the 'NCI60 data set', where applicable, one of the biological replicates was omitted while the remaining data constituted the training set.

Safety Considerations. To avoid any negative health impact originating from aerosolized cancer cells, the analysis site was enclosed into a Class II safety level glove box compartment equipped with UV light source and HEPA filters.

RESULTS AND DISCUSSION

Robustness of REIMS spectral profiles

REIMS analysis has been applied to different types of biological samples and showed good spectral pattern reproducibility in case of human tissues and microorganisms including both bacteria and fungi.[1,3] To test the general hypothesis that REIMS spectral patterns are reproducible and sufficiently specific to differentiate between different human cancer cell lines, three different cell lines (HeLa – cervical adenocarcinoma, MES-SA – uterine sarcoma, and SNB-19 – glioblastoma) were analyzed in an experiment designed to test spectral reproducibility. The experimental scheme depicted in Figure S-1 accounts for variance introduced by different culture batches or the passage number and for analytical variance introduced by the multiple measurements. Replicates were randomly analyzed over three analysis days in order to assess the analytical variance and robustness of a REIMS-based lipid profiling method. In addition, the influence of one freeze-thaw cycle on spectral variance was investigated and was found to be insignificant. Detailed sampling schedules can be found in Table S-2.

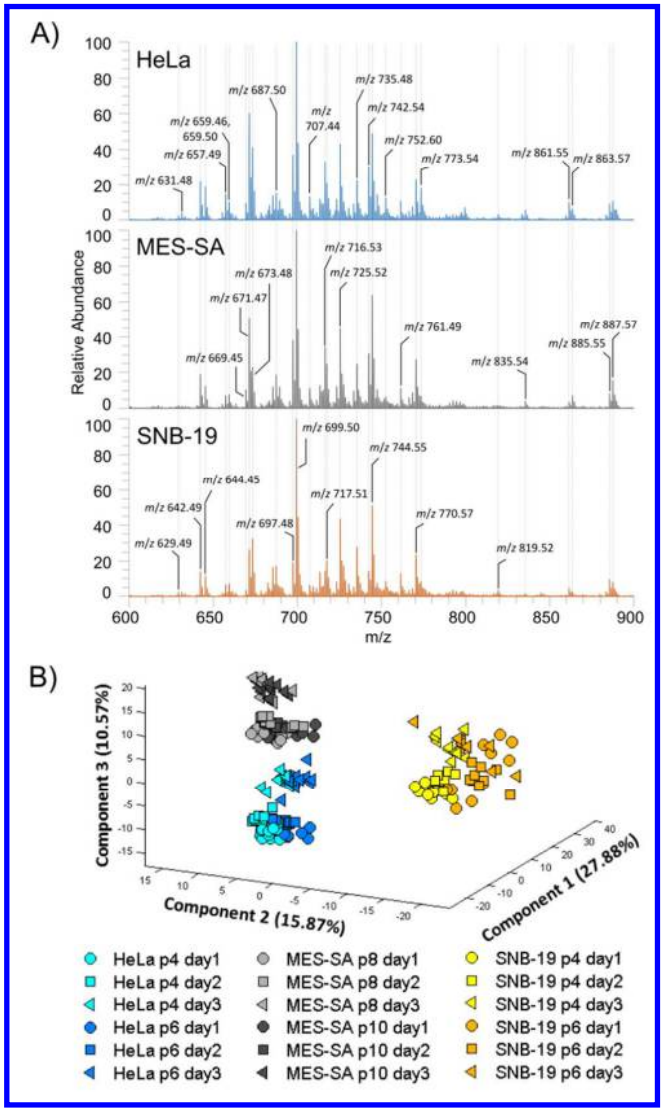

Figure 2. A) Representative mass spectral profiles between *m/z* 600-900 as obtained for HeLa, MES-SA, and SNB cell line pellets. B) 3-dimensional PCA plot of averaged REIMS data collected from several independent cultures of HeLa, MES-SA and SNB-19 cells over the spectral mass range of *m/z* 600-900.

Raw REIMS profiles of all three cell lines show a high degree of similarity (Figure 2A, see Figure S-3 for mass range of *m/z* 150-1000). Earlier studies demonstrated that REIMS is suitable to generate phospholipid profiles of various biological materials such as animal tissues,[2,27,28] human *ex-vivo* tissue samples of healthy and cancerous origin,[1,29] as well as microorganisms.[3,30] As analysis is performed in negative ion mode, the spectral content is similar to that described in those earlier studies featuring predominantly glycerophospholipid-type membrane lipids such as phosphatidylethanolamines

(PEs), phosphatidylinositols (PIs), phosphatidylglycerols (PGs), phosphatidic acids (PAs) and phosphatidylserines (PSs) as well as other complex lipids including ceramides and glycosylated ceramide species. All observed ions displayed a single negative charge, the vast majority by forming the quasi-molecular $[M-H]^-$ ion. In addition, $[M-NH_3-H]^-$ and $[M-NH_3+Cl]^-$ were observed in case of PEs. Sphingolipid species were detected as $[M+Cl]^-$ ions. A list of spectral features above a relative abundance of 2.5% with molecular assignments can be found in Table S-5. All identified spectral features were found to be lipids. The vast majority of lipid species detected using REIMS could also be detected in LC-MS measurements of the same cell lines (see Table S-5). For details about LC-MS sample preparation and instrument parameters the reader is referred to the Supplementary Information (Table S-3 and S-4).

For clinically oriented applications, REIMS spectral profiles were largely analyzed using supervised multivariate statistical methods such as linear discriminant analysis (LDA) to explore the differentiation of various tissue types or healthy and diseased tissues.[1,27] In this study, we intentionally restricted ourselves to exploratory unsupervised analysis methods to assess whether REIMS profiles would reproducibly cluster into different groups corresponding to cell line identities.

Table 1. Cross-validation results for SNB-19, HeLa and MES-SA cell lines based on a PCA model comprising the first 4 principal components and using 3 nearest neighbor as classifier.

Kept in test set	Predicted			Accuracy
	HeLa	MES-SA	SNB-19	
HeLa p6 A day2 (9 samples)	63	-	-	100%
MES-SA p8 A day1 (9 samples)	2	57	-	97%
SNB-19 p4 A day1 (9 samples)	-	-	54	100%
HeLa p4 B day2 (9 samples)	62	1	-	98%
MES-SA p10 B day1 (9 samples)	17	42	-	71%
SNB-19 p4 B day2 (7 samples)	-	-	56	100%
HeLa p4 A day1 (9 samples)	49	14	-	78%
MES-SA p10 A day3 (12 samples)	-	56	-	100%
SNB-19 p6 A day2 (7 samples)	-	1	55	98%

PCA of the REIMS profiles defined three clusters (Figure 2B), corresponding to the three cell lines. SNB-19 cells are clearly differentiated from HeLa and MES-SA cells along the first principal component. The second and the third principal component are required to fully separate HeLa and MES-SA cell lines from each other. A slight separation along the second principal component due to passage numbers was observed for HeLa and SNB-19, however, analytical and biological variances were found to be small compared to the inherent spectral differences of the cell lines. These results suggest that although there is an expected biological and analytical variance, the REIMS spectral profiles obtained from cell line pellets show sufficient reproducibility and specificity to characterize and distinguish human cancer cell lines.

Cross-validations were performed based on a PCA model created of training sets as described in Materials and Methods. Following this procedure, three different training sets were generated and subjected to PCA analysis. These training sets comprised between 25-28 sampling points, which represent <15% of the overall data points (n=203). The composition of the training sets and corresponding cross-validation results are shown in Table 1. Consistently, the cross-validation results show ≥98% correct classification for SNB-19 samples, with only a single misclassification observed in case of the third training set, which was tentatively associated with the unequal sample size for MES-SA (n=12) and SNB-19 (n=7). Unequal sample size is known to lead to a bias in PCA calculations towards the larger sample subset, which explains the misclassification of SNB-19 cells as MES-SA. While the first test set proved very robust for the classification of all three cell lines, the second and third test sets lead to occasional misclassifications between MES-SA and HeLa cells, respectively. This suggests a more close spectral relationship between HeLa (cervical origin) and MES-SA (uterine origin) compared to the SNB-19 cells (CNS origin) as was also observed in the PCA analysis as described above.

Significantly different m/z values were derived for all three cell lines using ANOVA in a one-against-all approach. Both significantly increased and significantly decreased *m*/*z* values can be found in Table S-6. Similar trends for these significantly changed species are shown for the same three cell lines using LC-MS measurements (see Figure S-2 for box plots derived from either methodology).

REIMS profile of the NCI60 cell line panel

Following the confirmation that REIMS spectral patterns are able to distinguish between three cancer cell lines, we set out to profile the entire NCI60 panel, consisting of 60 human different cancer cell lines. Based on amount of available biomass after culture, we recorded 4 to 15 individual measurement points for each cell line, and included eight biological replicates (see Table S-7 for detailed sample set). Hierarchical cluster analysis (HCA; Figure 3) and principal component analysis (Figure S-4) of the filtered spectral averages were performed. The spectral content of the different cell lines was compared and no mass spectrometric signals were unique for a single cell line only. Rather, changes in lipid content were of a relative nature and clustering behavior of cell lines was due to pattern-level changes rather than changes in the relative intensity of a few species. Biological replicates showed the expected level of similarity as indicated by the cluster analysis (Figure 3) showing close clustering in the HCA dendrogram. This is true for all cell lines except

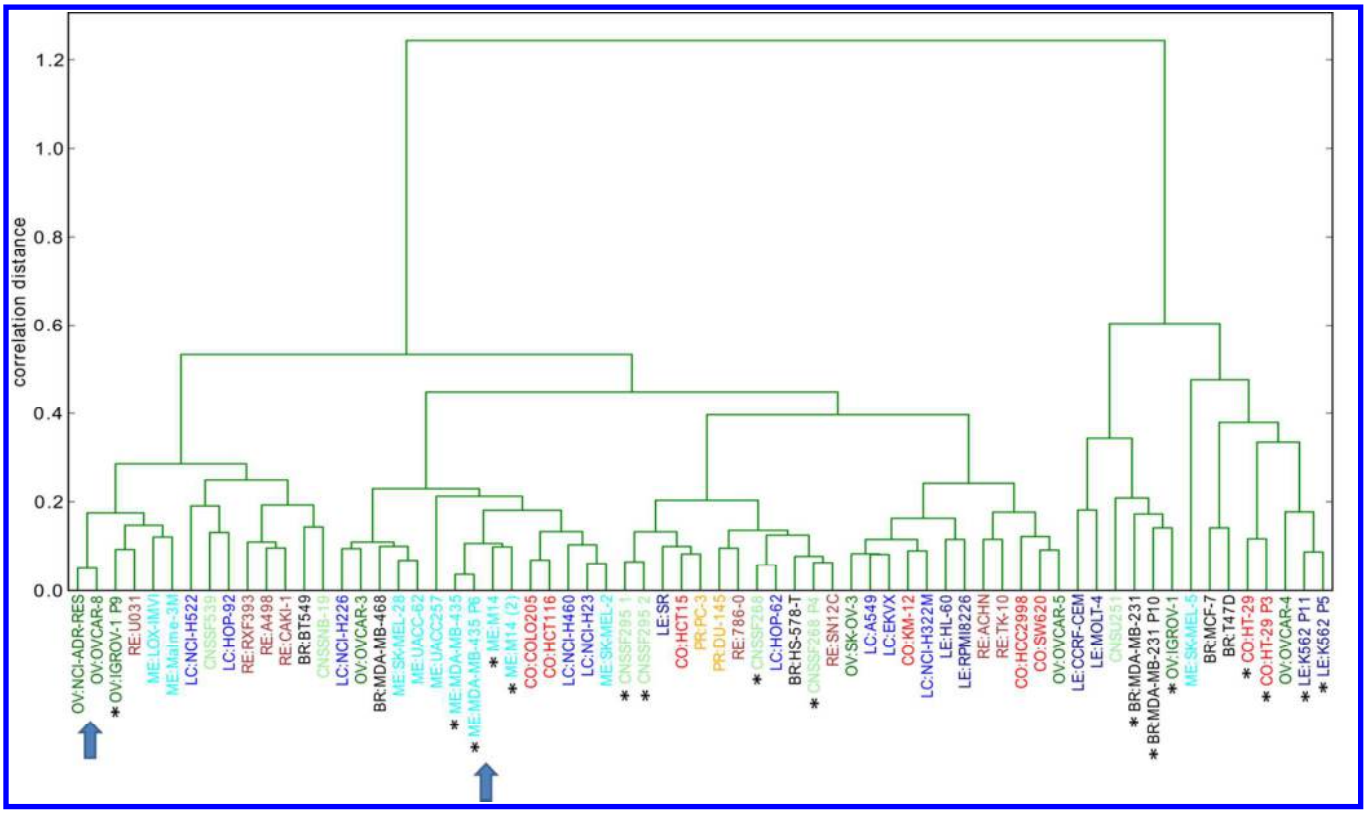

Figure 3. Cluster dendrogram of the NCI60 panel including independently cultured replicates (highlighted by asterisks) or biologically related cell lines (blue arrows). REIMS lipidomic profiles distinguish cell lines of the NCI60 panel consisting of ovarian (OV, green), renal (RE, brown), melanoma (ME, light blue), central nervous system (CNS, light green), breast (BR, black), lung (LC, blue), colon (CO, red), leukemia (LE, purple) and prostate (PR, yellow) origin. Distance was calculated using Pearson correlation and agglomeration via the Ward metric.

IGROV-1 and SF-268. In case of IGROV-1, a comparably small number of 3 and 5 REIMS spectra were available for each respective replicate, which was tentatively associated with the incorrect classification. The spectral difference observed in the case of SF-268 raises the possibility of strong biological variance or a potentially compromised biological replicate. Similar results were obtained for cross-validation results performed on the PCA model (see Table S-8 for identification accuracies based on PCA model shown in Figure S-4) which reveal partial misclassification for IGROV-1 and no correct results for SF-268.

Gene expression profiling revealed that the MDA-MB-435 cells more closely resembled melanoma cell lines than the other breast tumor lines.[31] Consistent with gene expression,[32] SNP[33] and karyotype analyses,[34] the REIMS profiles also indicate that MDA-MB-435 and M14 are closely related (Figure 3, blue arrow, right). Karyotyping has also found that NCI-ADR-RES is in fact a drug-resistant derivative of OVCAR-8.[35] As shown in Figure 3, these cell lines (indicated by blue arrow, left) also show close similarity based on their REIMS profiles. Taken together, these results confirm that REIMS profiles are strongly associated with the biological identity of cancer cell lines. Gene and protein expression patterns of the NCI-60 panel were found to correlate with tissue type of origin to some extent,[12,32] whereas metabolic signatures did not differentiate well between tissue origins.[14] Clustering of the cell lines based on their REIMS lipid profile showed extensive heterogeneity within most tissue types, except for melanoma samples (Figure 3, light blue colored cell lines).

In previous studies, the REIMS spectral profile of *ex-vivo* human tissue specimens was shown to be highly specific for the histological/anatomical tissue type.[1] REIMS profiles of the NCI60 panel were subsequently compared to bulk cancer samples of ovarian and colon adenocarcinomas analyzed using the same experimental setup. A PCA plot of the resulting dataset is shown in Figure 4A and reveals clear differences between cell lines and bulk tissue specimens along the first principal component suggesting strong differences among their membrane lipid composition. A tentative separation according to tissue type of origin can be observed for both cell lines and tissue specimens, although more pronounced in the latter. Only a small number of tissue specimens (n=4) were available in case of ovarian tumors, but based on previous studies a significant increase in separation power can be expected for larger sample sets.[1] Nevertheless, the direction of separation is similar in both cases, suggesting similar lipidomic differences.

Representative spectral profiles in the mass range of 600-900Da of both ovarian and colon cancer tissue and cell line samples are shown in Figure 4B (see Figure S-5 for REIMS spectral profiles ranging from 150-1000Da). Significantly different *m/z* values between bulk tissues and cell lines of the same tissue of origin were derived using ANOVA and are shown in Table S-9. Box plots for representative *m/z* species are shown in Figure S-6. Bulk tissues display larger amounts of long-chain phosphatidylinositols such as PI(38:4) at *m/z* 885.55. Similar trends were observed in case of certain phosphatidylethanolamines, for instance the peaks detected in the mass range of *m/z* 790-794 corresponding to PE(40:6)-

PE(40:4) species or those occurring at *m/z* 766.54 and 768.55 corresponding to PE(38:4) and PE(38:3), respectively. On the other hand, predominantly shorter chain PEs and PAs with 30-36 cumulative carbon chain lengths were found to be more abundant in cell lines. We speculate that the characteristic differences in lipid composition are due to the uniform lipid content of the culturing medium, which does not recapitulate the complex lipid source of real tumors that rely on dietary and liver-synthesized lipids as well as *de-novo* lipid synthesis.

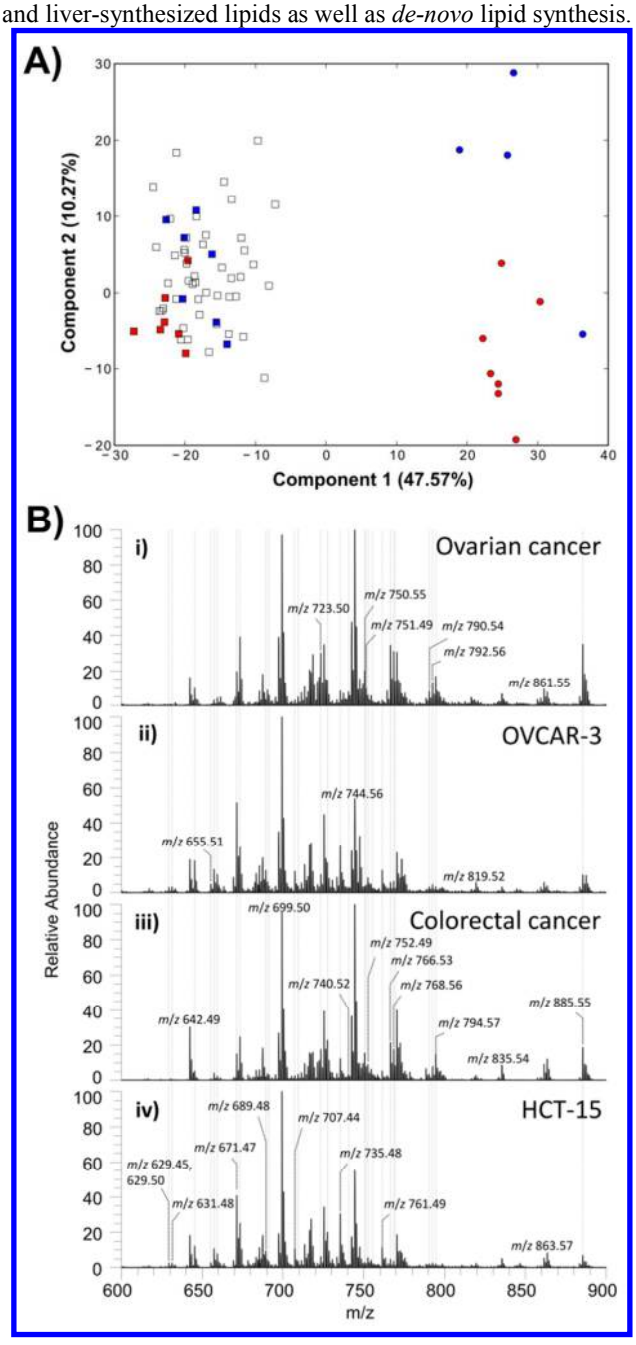

Figure 4. A) 2-dimensional PCA plot of REIMS data collected from the NCI60 cells (squares) and cancer tissue samples (circles). The tissue of origin is indicated by red (colon) and blue (ovarian) colors. B) Comparison of spectral profiles for bulk tissue samples and cell lines of the corresponding tissue type of origin for i) ovarian cancer and ii) OVCAR-3 cell line, iii) colorectal cancer and iv) HCT-15 cell line.

Analysis of Mycoplasma-infected cell lines

Mycoplasma contamination is a major problem in both basic and applied research. Infection with Mycoplasma alters many physiological processes and often confounds experimental results. Plasmocin™ (InvivoGen, San Diego, CA, USA) is a commercially available antibiotic treatment that is frequently used to eradicate Mycoplasma infection in cell cultures.[36]

REIMS profiles of Mycoplasma-free, Mycoplasma-infected and Plasmocin™-treated HEK and HeLa cell lines were recorded. The dataset was pre-processed as described for the NCI60 panel. Our aim was to identify *m/z* values showing significantly different intensity between Mycoplasma-positive and -negative samples. Adjusted p-values were obtained using the adaptive Benjamini–Hochberg (BH) procedure to correct for multiple testing.[37] As shown in Figure 5A, 23 and 386 binned *m/z* signals were significantly higher in Mycoplasma-infected HEK and HeLa cells, respectively. The higher number of significantly increased peaks found for HeLa cells may be explained with a higher number of sampling points (contributing to higher power in significance testing) or may reflect the increased reactivity of HeLa cells to Mycoplasma infection. Interestingly, we found only one signal showing reduced intensity in Mycoplasma-infected cell lines. Table S-10 lists the tentative annotation of the 18 *m/z* signals that were found to be significantly increased across all Mycoplasma-infected cells.

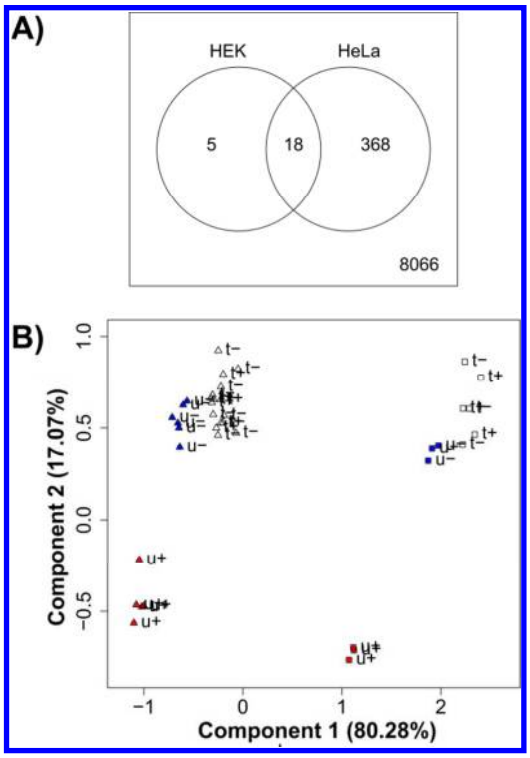

Figure 5. A) Number of significantly higher *m/z* signals in Mycoplasma-infected versus Mycoplasma-free samples in HEK and HeLa cell lines. B) Mycplasma-infected (+) and Mycoplasma-free (-) HEK (rectangle) and HeLa (triangle) cells that were either treated (t) or untreated (u). Samples are shown as a function of PC1 and PC2 of PCA transformed data points in the space of the 18 overlapping *m/z* signals.

As an example, changes in the intensity of *m/z* 819.52 (identified as PG(40:7) based on exact mass measurements) are shown in Mycoplasma-free, Mycoplasma-infected and Plasmocin™-treated HEK and HeLa cells (Figure S-7). This *m/z* value, along with the signal corresponding to its isotope, was found to be increased in Mycoplasma-infected HeLA and HEK cells, whereas the intensity returned to pre-infection levels upon successful Plasmocin™ treatment. Similar results were obtained for the other *m/z* signals listed in Table S-10.

In the 18 dimensional space of these *m/z* signals, Mycoplasma-infected and Mycoplasma-free HEK and HeLa samples were analyzed by PCA (Figure 5B). The first principal component (PC1) reveals differences between the two different cell lines while the second PC separates Mycoplasma-free and Mycoplasma-infected samples. The significantly increased signals correspond to phosphoglycerolipids that are however also present in healthy cell lines, suggesting that the changes delineated by the statistical analysis are not due to the presence of bacterial lipids. Rather, we speculate that the peaks showing increased intensity reflect changes that are associated with the reversible response of the host cells' lipid metabolism to Mycoplasma infection.[38] Our results indicate that REIMS analysis can identify spectral changes evoked by Mycoplasma infection. Future studies will delineate the complex effect of Mycoplasma infection on the lipidomic profiles of cell lines and reveal the applicability of the REIMS technology in the rapid and reliable detection of Mycoplasma infection.

CONCLUSION

This proof-of-principle study demonstrates the applicability of a REIMS-based shotgun lipidomic characterization approach for human cancerous cell lines. Individual cancer cell lines were found to exhibit reproducible and cell line-specific spectral profiles while spectra could be acquired in less than five seconds. REIMS analysis does not only allow rapid identification of cell lines based on their spectral fingerprint, but opens the way to the detailed characterization of membrane lipid composition in different cancer phenotypes. The correlation between REIMS spectral data and gene and protein expression data can be assessed using publicly available resources such as the CellMiner database [39] which will allow to assess the sensitivity of the REIMS spectral method for tumor phenotypic characterization in detail. In addition, this technique offers a unique possibility to investigate gene knock-out models for changes in lipid metabolism or the effects of feeding experiments with stable isotope-labeled nutrient sources.

ASSOCIATED CONTENT

Supporting Information Available: More detailed information on experimental setup and instrument parameters for REIMS and LC-MS analyses, sample size and composition used, results of further multivariate and univariate analyses, lists of significant spectral features for reproducibility, cell vs bulk and mycoplasma sample sets. This material is available free of charge via the Internet at http://pubs.acs.org.

AUTHOR INFORMATION

Corresponding Author

*Prof. Zoltan Takats, Department of Surgery and Cancer, Sir Alexander Fleming Building, Imperial College, London SW7 2AZ, United Kingdom. Tel: +44 (0)207 5942760; E-mail: z.takats@imperial.ac.uk.

*Dr. Gergely Szakacs, Institute of Enzymology, Research Centre for Natural Sciences, Hungarian Academy of Sciences, Budapest 1117, Hungary. Tel: +36 1 382 6715, E-mail: szakacs.gergely@ttk.mta.hu.

Present Address

† Drug Safety and Metabolism, AstraZeneca, Cambridge, UK.

Author Contributions

Study was planned by ZT, GS, AL and NS. Cell lines were prepared by NK. Experiments were conducted by NS. Data was analyzed and interpreted by NS, AL, JS, JSM, ZT and GS. Manuscript was revised by NS, AL, GS, ZB, MLD, ZT. The manuscript was written through contributions of all authors. All authors have given approval to the final version of the manuscript.

‡These authors contributed equally.

Conflict of Interest Disclosure

The authors declare no competing financial interest.

ACKNOWLEDGMENT

The work was funded by the European Research Council under the Starting Grant scheme (Contract No. 210356) the European commission FP7 intelligent surgical device project (Contract No. 3054940) and the European Research Council Consolidator Grant scheme (Contract No. 617896). GS was supported by a Momentum Grant of the Hungarian Academy of Sciences.

REFERENCES

(1) Balog, J.; Sasi-Szabo, L.; Kinross, J.; Lewis, M. R.; Muirhead, L. J.; Veselkov, K.; Mirnezami, R.; Dezso, B.; Damjanovich, L.; Darzi, A.; Nicholson, J. K.; Takats, Z. *Sci Transl Med* **2013**, *5*, 194ra193.

(2) Schafer, K. C.; Denes, J.; Albrecht, K.; Szaniszlo, T.; Balog, J.; Skoumal, R.; Katona, M.; Toth, M.; Balogh, L.; Takats, Z. *Angew Chem Int Ed* **2009**, *48*, 8240-8242.

(3) Strittmatter, N.; Rebec, M.; Jones, E. A.; Golf, O.; Abdolrasouli, A.; Balog, J.; Behrends, V.; Veselkov, K. A.; Takats, Z. *Anal Chem* **2014**, *86*, 6555-6562.

(4) Chingin, K.; Liang, J.; Chen, H. *RSC Adv* **2014**, *4*, 5768-5781.

(5) Takáts, Z.; Wiseman, J. M.; Gologan, B.; Cooks, R. G. *Science* **2004**, *306*, 471-473.

(6) Takats, Z.; Cotte-Rodriguez, I.; Talaty, N.; Chen, H.; Cooks, R. G. *Chem Commun* **2005**, 1950-1952.

(7) Calligaris, D.; Caragacianu, D.; Liu, X.; Norton, I.; Thompson, C. J.; Richardson, A. L.; Golshan, M.; Easterling, M. L.; Santagata, S.; Dillon, D. A.; Jolesz, F. A.; Agar, N. Y. R. *Proc Nat Acad Sci* **2014**, *111*, 15184-15189.

(8) Abbassi-Ghadi, N.; Veselkov, K.; Kumar, S.; Huang, J.; Jones, E.; Strittmatter, N.; Kudo, H.; Goldin, R.; Takats, Z.; Hanna, G. B. *Chem Commun* **2014**, *50*, 3661-3664.

(9) Gerbig, S.; Golf, O.; Balog, J.; Denes, J.; Baranyai, Z.; Zarand, A.; Raso, E.; Timar, J.; Takats, Z. *Anal Bioanal Chem* **2012**, *403*, 2315-2325.
(10) Eberlin, L. S.; Norton, I.; Orringer, D.; Dunn, I. F.; Liu, X.; Ide, J. L.; Jarmusch, A. K.; Ligon, K. L.; Jolesz, F. A.; Golby, A. J.; Santagata, S.; Agar, N. Y. R.; Cooks, R. G. *Proc Nat Acad Sci* **2013**, *110*, 1611-1616.
(11) Shoemaker, R. H. *Nat Rev Can* **2006**, *6*, 813-823.
(12) Gholami, Amin M.; Hahne, H.; Wu, Z.; Auer, Florian J.; Meng, C.; Wilhelm, M.; Kuster, B. *Cell Rep* **2013**, *4*, 609-620.
(13) Ikediobi, O. N.; Davies, H.; Bignell, G.; Edkins, S.; Stevens, C.; O'Meara, S.; Santarius, T.; Avis, T.; Barthorpe, S.; Brackenbury, L.; Buck, G.; Butler, A.; Clements, J.; Cole, J.; Dicks, E.; Forbes, S.; Gray, K.; Halliday, K.; Harrison, R.; Hills, K.; Hinton, J.; Hunter, C.; Jenkinson, A.; Jones, D.; Kosmidou, V.; Lugg, R.; Menzies, A.; Mironenko, T.; Parker, A.; Perry, J.; Raine, K.; Richardson, D.; Shepherd, R.; Small, A.; Smith, R.; Solomon, H.; Stephens, P.; Teague, J.; Tofts, C.; Varian, J.; Webb, T.; West, S.; Widaa, S.; Yates, A.; Reinhold, W.; Weinstein, J. N.; Stratton, M. R.; Futreal, P. A.; Wooster, R. *Mol Can Ther* **2006**, *5*, 2606-2612.
(14) Su, G.; Burant, C. F.; Beecher, C. W.; Athey, B. D.; Meng, F. *BMC Bioinform* **2011**, *12 Suppl 1*, S36.
(15) Doria, M. L.; Cotrim, C. Z.; Simoes, C.; Macedo, B.; Domingues, P.; Domingues, M. R.; Helguero, L. A. *J Cell Phys* **2013**, *228*, 457-468.
(16) Fillet, M.; Van Heugen, J. C.; Servais, A. C.; De Graeve, J.; Crommen, J. *J Chrom A* **2002**, *949*, 225-233.
(17) Bodzon-Kulakowska, A.; Cichon, T.; Golec, A.; Drabik, A.; Ner, J.; Suder, P. *Cytotechnology* **2015**, *67*, 1085-1091.
(18) Fhaner, C. J.; Liu, S.; Ji, H.; Simpson, R. J.; Reid, G. E. *Anal Chem* **2012**, *84*, 8917-8926.
(19) Shrestha, B.; Sripadi, P.; Walsh, C. M.; Razunguzwa, T. T.; Powell, M. J.; Kehn-Hall, K.; Kashanchi, F.; Vertes, A. *Chem Commun* **2012**, *48*, 3700-3702.
(20) Sripadi, P.; Shrestha, B.; Easley, R. L.; Carpio, L.; Kehn-Hall, K.; Chevalier, S.; Mahieux, R.; Kashanchi, F.; Vertes, A. *PLoS ONE* **2010**, *5*, e12590.
(21) Dória, M. L.; Cotrim, Z.; Macedo, B.; Simões, C.; Domingues, P.; Helguero, L.; Domingues, M. R. *Breast Can Res Treat* **2012**, *133*, 635.
(22) Yu, Y.; Vidalino, L.; Anesi, A.; Macchi, P.; Guella, G. *Mol BioSys* **2014**, *10*, 878-890.
(23) Chambers, M. C.; Maclean, B.; Burke, R.; Amodei, D.; Ruderman, D. L.; Neumann, S.; Gatto, L.; Fischer, B.; Pratt, B.; Egertson, J.; Hoff, K.; Kessner, D.; Tasman, N.; Shulman, N.; Frewen, B.; Baker, T. A.; Brusniak, M. Y.; Paulse, C.; Creasy, D.; Flashner, L.; Kani, K.; Moulding, C.; Seymour, S. L.; Nuwaysir, L. M.; Lefebvre, B.; Kuhlmann, F.; Roark, J.; Rainer, P.; Detlev, S.; Hemenway, T.; Huhmer, A.; Langridge, J.; Connolly, B.; Chadick, T.; Holly, K.; Eckels, J.; Deutsch, E. W.; Moritz, R. L.; Katz, J. E.; Agus, D. B.; MacCoss, M.; Tabb, D. L.; Mallick, P. *Nat Biotech* **2012**, *30*, 918-920.
(24) Race, A. M.; Styles, I. B.; Bunch, J. *J Proteomics* **2012**, *75*, 5111-5112.
(25) Veselkov, K. A.; Lindon, J. C.; Ebbels, T. M. D.; Crockford, D.; Volynkin, V. V.; Holmes, E.; Davies, D. B.; Nicholson, J. K. *Anal Chem* **2009**, *81*, 56-66.
(26) Ihaka, R.; Gentleman, R. *J Comp Graph Stat* **1996**, *5*, 299-314.
(27) Balog, J.; Szaniszlo, T.; Schaefer, K.-C.; Denes, J.; Lopata, A.; Godorhazy, L.; Szalay, D.; Balogh, L.; Sasi-Szabo, L.; Toth, M.; Takats, Z. *Anal Chem* **2010**, *82*, 7343-7350.
(28) Golf, O.; Muirhead, L. J.; Speller, A.; Balog, J.; Abbassi-Ghadi, N.; Kumar, S.; Mróz, A.; Veselkov, K.; Takáts, Z. *J Am Soc Mass Spectrom* **2014**, *26*, 44-54.
(29) Balog, J.; Kumar, S.; Alexander, J.; Golf, O.; Huang, J.; Wiggins, T.; Abbassi-Ghadi, N.; Enyedi, A.; Kacska, S.; Kinross, J.; Hanna, G. B.; Nicholson, J. K.; Takats, Z. *Angew Chem Int Ed* **2015**, *54*, 11059-11062.
(30) Strittmatter, N.; Jones, E. A.; Veselkov, K. A.; Rebec, M.; Bundy, J. G.; Takats, Z. *Chem Commun* **2013**, *49*, 6188-6190.
(31) Ross, D. T.; Scherf, U.; Eisen, M. B.; Perou, C. M.; Rees, C.; Spellman, P.; Iyer, V.; Jeffrey, S. S.; Van de Rijn, M.; Waltham, M.; Pergamenschikov, A.; Lee, J. C. F.; Lashkari, D.; Shalon, D.; Myers, T. G.; Weinstein, J. N.; Botstein, D.; Brown, P. O. *Nat Genet* **2000**, *24*, 227-235.
(32) Scherf, U.; Ross, D. T.; Waltham, M.; Smith, L. H.; Lee, J. K.; Tanabe, L.; Kohn, K. W.; Reinhold, W. C.; Myers, T. G.; Andrews, D. T.; Scudiero, D. A.; Eisen, M. B.; Sausville, E. A.; Pommier, Y.; Botstein, D.; Brown, P. O.; Weinstein, J. N. *Nat Genet* **2000**, *24*, 236-244.
(33) Garraway, L. A.; Widlund, H. R.; Rubin, M. A.; Getz, G.; Berger, A. J.; Ramaswamy, S.; Beroukhim, R.; Milner, D. A.; Granter, S. R.; Du, J.; Lee, C.; Wagner, S. N.; Li, C.; Golub, T. R.; Rimm, D. L.; Meyerson, M. L.; Fisher, D. E.; Sellers, W. R. *Nature* **2005**, *436*, 117-122.
(34) Rae, J. M.; Creighton, C. J.; Meck, J. M.; Haddad, B. R.; Johnson, M. D. *Breast Can Res Treat* **2007**, *104*, 13-19.
(35) Liscovitch, M.; Ravid, D. *Cancer letters* **2007**, *245*, 350-352.
(36) Uphoff, C. C.; Denkmann, S. A.; Drexler, H. G. *J Biomed Biotech* **2012**, *2012*, 267678.
(37) Benjamini, Y.; Hochberg, Y. *J Educ Behav Stat* **2000**, *25*, 60-83.
(38) Drexler, H.; Uphoff, C. *Cytotechnology* **2002**, *39*, 75-90.
(39) Shankavaram, U. T.; Varma, S.; Kane, D.; Sunshine, M.; Chary, K. K.; Reinhold, W. C.; Pommier, Y.; Weinstein, J. N. *BMC Genomics* **2009**, *10*, 277.

TABLE OF CONTENT